A Consistent Sea-Level Reconstruction and Its Budget on Basin and Global Scales over 1958–2014

THOMAS FREDERIKSE

Department of Geoscience and Remote Sensing, Delft University of Technology, Delft, Netherlands

SVETLANA JEVREJEVA

National Oceanography Centre, Liverpool, United Kingdom

RICCARDO E. M. RIVA

Department of Geoscience and Remote Sensing, Delft University of Technology, Netherlands

SÖNKE DANGENDORF

Research Institute for Water and Environment, University of Siegen, Siegen, Germany

(Manuscript received 27 July 2017, in final form 31 October 2017)

ABSTRACT

Different sea level reconstructions show a spread in sea level rise over the last six decades and it is not yet certain whether the sum of contributors explains the reconstructed rise. Possible causes for this spread are, among others, vertical land motion at tide-gauge locations and the sparse sampling of the spatially variable ocean. To assess these open questions, reconstructed sea level and the role of the contributors are investigated on a local, basin, and global scale. High-latitude seas are excluded. Tide-gauge records are combined with observations of vertical land motion, independent estimates of ice-mass loss, terrestrial water storage, and barotropic atmospheric forcing in a self-consistent framework to reconstruct sea level changes on basin and global scales, which are compared to the estimated sum of contributing processes. For the first time, it is shown that for most basins the reconstructed sea level trend and acceleration can be explained by the sum of contributors, as well as a large part of the decadal variability. The sparsely sampled South Atlantic Ocean forms an exception. The global-mean sea level reconstruction shows a trend of $1.5 \pm 0.2\,\mathrm{mm\,yr^{-1}}$ over 1958–2014 (1σ), compared to $1.3 \pm 0.1\,\mathrm{mm\,yr^{-1}}$ for the sum of contributors. Over the same period, the reconstruction shows a positive acceleration of $0.07 \pm 0.02\,\mathrm{mm\,yr^{-2}}$, which is also in agreement with the sum of contributors, which shows an acceleration of $0.07 \pm 0.01\,\mathrm{mm\,yr^{-2}}$. Since 1993, both reconstructed sea level and the sum of contributors show good agreement with altimetry estimates.

1. Introduction

Global sea level reconstructions before the satellite altimetry era mostly depend on tide-gauge records, which are sparsely sampled over the globe, contain data gaps, and are affected by vertical land motion (VLM). These problems pose a challenge for reconstructions of global and regional sea level rise. A wide variety of methods has been used to reconstruct global sea level changes from individual tide-gauge records. These methodological differences, together with the inclusion or exclusion of specific tide-gauge stations, result in a large spread in published sea level rise estimates. As an example, the mean estimates of sea level rise from 1900 to 1990 vary between 1.1 and $2.0\,\mathrm{mm\,yr^{-1}}$ (Church and White 2011; Jevrejeva et al. 2014; Hay et al. 2015; Dangendorf et al. 2017). This large spread in reconstructed sea level trends hinders the attribution of observed sea level changes to the individual processes. Over the twentieth century, Gregory et al. (2013) and Slangen et al. (2016) find that the sum of contributors,

Supplemental information related to this paper is available at the Journals Online website: https://doi.org/10.1175/JCLI-D-17-0502.s1.

Corresponding author: Thomas Frederikse, t.frederikse@tudelft.nl

DOI: 10.1175/JCLI-D-17-0502.1

based on climate model results, is lower than the observed rise in global mean sea level. The latter study denotes that the largest difference occurs during 1940–70. Consequently, most estimates (both modeled and observed) of the contributors over the second half of the twentieth century fail to explain the available observations (Moore et al. 2011). Only after 1971 and during the altimetry era can the sea level budget be reasonably closed (Church et al. 2011; Chambers et al. 2017). It is not yet known whether this budget gap before the 1970s is present in all ocean regions or if it is only present in some areas. To our knowledge, the only study before the satellite era that discusses this problem is from Slangen et al. (2014), who also find a budget gap on a global scale, but cannot find specific regions to which this gap can be linked.

Recently, two new global sea level reconstructions point at substantially lower sea level changes before 1990 (Hay et al. 2015; Dangendorf et al. 2017). In these reconstructions, known information about the spatial patterns of VLM and sea level rise and, in the latter study, direct VLM observations have been explicitly taken into account. The tide-gauge selection criteria have a profound impact on the resulting sea level curve (Hamlington and Thompson 2015). However, the addition of prior knowledge of these spatial patterns results in a sea level curve that is more robust to the tide-gauge selection criteria (Hay et al. 2017; Dangendorf et al. 2017).

Whether these new sea level curves are in agreement with the observations of the contributors is an open question, and it is not yet clear whether this addition of knowledge about local VLM and spatial patterns affects the sea level budget on a regional scale.

To answer these questions, a new reconstruction technique is proposed that takes the spatial sea level variability associated with glacial isostatic adjustment (GIA) and present-day mass redistribution into account, as well as local VLM at the tide-gauge location. Based on the results of Thompson and Merrifield (2014), we have divided the global ocean into six regions, which share a common signal of decadal sea level variability. We reconstruct sea level in each basin, as well as for the global ocean, and compare the reconstructions to the sum of contributors. This comparison on a basin scale also enables us to directly identify particularly critical regions.

Nowadays, robust estimates of local VLM at tide gauges are available from continuous GPS receivers and from the difference between satellite altimetry and tide-gauge observations (Wöppelmann and Marcos 2016). These estimates have generated a more homogeneous picture of regional sea level estimates (Wöppelmann et al. 2009). While traditionally only the GIA component of VLM was removed in global sea level reconstructions, recent studies point toward a bias in GMSL when the VLM signal is not taken into account (Hamlington et al. 2016; Dangendorf et al. 2017). However, estimates of VLM are usually based on GPS series of much shorter duration than the tide-gauge records in use, leading to the formerly necessary assumption that they can be linearly extrapolated back in time. This assumption holds for long-term contributions as GIA, but certainly fails for most processes related to present-day mass transport. For instance, present-day ice-mass loss and terrestrial freshwater sources are highly nonlinear and partly contain accelerating components, which affect relative sea level, but also the height of the solid earth surface (Tamisiea 2011; Riva et al. 2017). To circumvent this resulting bias, we use the modeling framework from Frederikse et al. (2016, 2017), in which the observed VLM is separated into a part explained by present-day mass redistribution and GIA, constrained by forward models, and an unexplained part, constrained by direct VLM observations.

This paper is structured as follows: the tide-gauge selection and VLM observations are discussed in section 2. In section 3, we discuss the modeled and observed individual contributors to local, regional, and global sea level changes. The local sea level and VLM observations are compared to the sum of contributors in section 4. The reconstruction of basin-mean and global sea level and the comparison with the sum of contributors are discussed in section 5, followed by the discussion and conclusions.

2. Tide-gauge data and vertical land motion estimates

Monthly-mean tide-gauge observations have been obtained from the Permanent Service for Mean Sea Level (PSMSL; Holgate et al. 2013). VLM observations are either computed from nearby permanent GPS stations or from the difference between tide-gauge and altimetry observations. A list of collocated GPS and tide-gauge locations has been obtained from SONEL (Systeme d'Observation du Niveau des Eaux Littorales; www.sonel.org). GPS observations of VLM have been obtained from Nevada Geodetic Laboratory, for which trends and the accompanying uncertainty have been estimated using the median interannual difference adjusted for skewness (MIDAS) method (Blewitt et al. 2016). VLM estimates based on altimetry minus tide-gauge observations are the same as in Wöppelmann and Marcos (2016). We have selected stations for which at least 240 monthly-mean sea level observations are

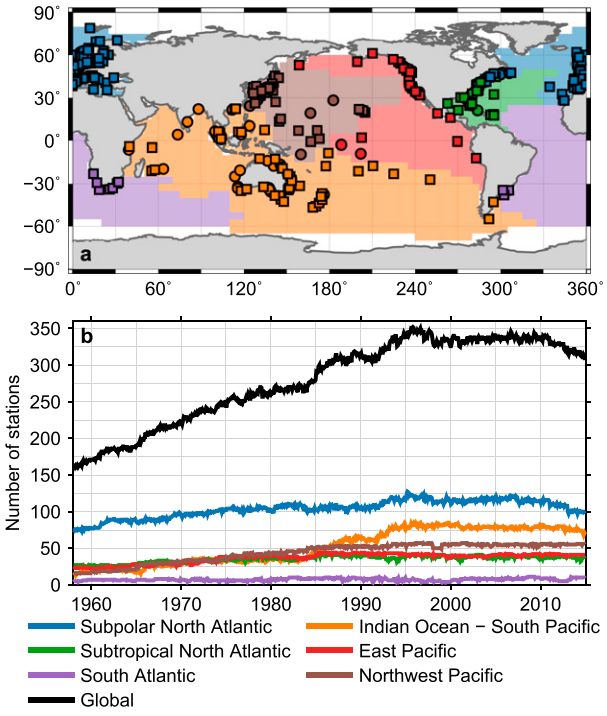

FIG. 1. Stations and ocean basins used in this study. (a) Location of each tide-gauge station and the definition of each ocean basin. The color of the dots depict the region to which each tide gauge is tied to. Square dots denote tide gauges for which VLM is determined from GPS observations, while circles denote stations for which altimetry minus tide-gauge data is used to determine VLM. (b) Number of stations per basin that have data in each month.

available, for which the error on the VLM trend is smaller than 2 mm yr^{-1} and for which the difference between the observed trend and the sum of individual processes, defined in Eq. (3), is smaller than 3 mm yr^{-1}. Furthermore, we have excluded the station Ilha Fiscal along the western boundary of the South Atlantic, since this station shows a very strong multidecadal variability pattern that is unlikely to be related to large-scale patterns. This station has also been ignored in the reconstructions of Church and White (2011) and Dangendorf et al. (2017). With these selection criteria, we obtain 396 individual tide-gauge stations. For station locations for which multiple GPS observations are available, the total trend is computed as the mean of the individual GPS stations, weighted by the inverse of the standard error of each individual trend.

For estimates of basin-mean sea level, we distinguish six ocean basins, based on the regions defined in Thompson and Merrifield (2014), who found a coherent decadal sea level variability signal in each region. Each tide-gauge station is linked to a specific basin. Figure 1a shows the locations of the selected tide-gauge stations, the method to estimate VLM, as well as the ocean basins to which each station is linked. In the figure, it can be seen that the ocean basins in Northern Hemisphere have comparably high data coverage, while the South Atlantic basin is only sparsely covered: the African and South American coasts only have a few records, and no long-term records from open-ocean islands are available in this basin. The availability of station data per month is depicted in Fig. 1b. For all basins, except for the South Atlantic region, for which only a few tide-gauge observations are available, observations come from at least 10 stations during any time of the analysis. A table with all individual tide-gauge stations and the method used to estimate local VLM can be found in the supplemental information. The ocean basins do not cover parts of the Arctic and Southern Oceans. These uncovered areas, which are shown in white in Fig. 1a, form 7% of the global oceans. In this study, we do not include these areas, and where we use the word "global," we mean the total area covered by the six aforementioned ocean basins, excluding the white parts in Fig. 1a.

Local barotropic effects due to wind and sea level pressure changes can have a profound impact on local sea level variability, even on longer time scales (e.g., Dangendorf et al. 2013; Piecuch et al. 2016). Since these signals are generally not basinwide in origin, we estimate and remove this signal by using a simple linear regression model, similar to Frederikse et al. (2016) and Frederikse et al. (2017). The regression model contains an annual cycle, semiannual cycle, wind stress in the zonal and meridional direction, and the local deviation from the ocean-mean sea level pressure. Pressure and wind fields are obtained from the Twentieth Century Reanalysis (20CR; Compo et al. 2011) and, for each tide-gauge station, the model grid point with the highest correlation with local sea level within a radius of 250 km is used. The signals related to wind and pressure are only removed if the regression coefficient is significantly different from zero at the 2σ level, which is tested using a t-test statistic.

After removing local barotropic effects, we compute linear trends in sea level and VLM at each tide-gauge location. These trends are displayed in Fig. 2. The figure shows that at most stations the sea level trend is positive, with some regions having a common signal: the trends along the U.S. East Coast and around Australia appear to be high, while at the U.S. West Coast the trends appear to be almost zero. The VLM trends are generally smaller, and have less profound regional signals, except for the positive VLM trends at the western U.S. coast, which may partially explain the low trends in that region, and the uplift around northern Europe, which is to a large extent caused by GIA (Hill et al. 2010).

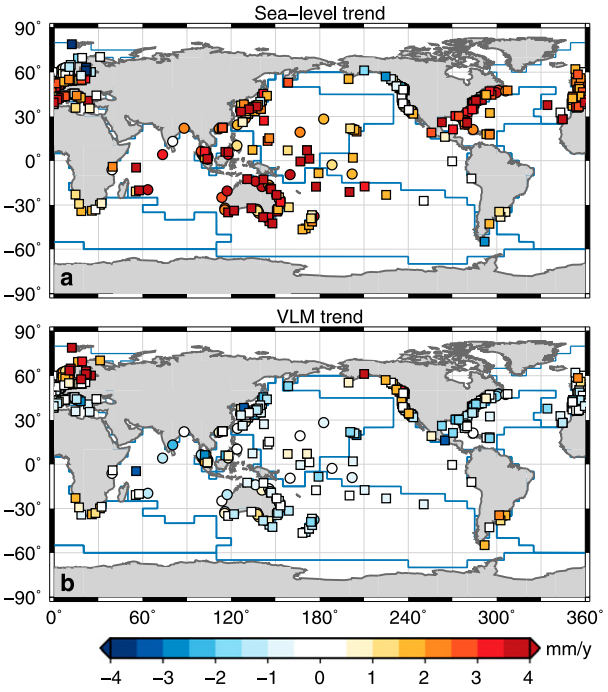

FIG. 2. Linear trends at individual tide-gauge locations. (a) Trend in relative sea level over available data within 1958–2014. The local barotropic effects of wind and pressure were removed using the regression model before computing the trend. (b) Linear trends in VLM. The blue line depict the boundaries of the ocean basins. Note that, given the availability of observations, the period over which the trends are computed differs between stations.

We use satellite altimetry to compare our tide-gauge reconstruction to independent observations. Gridded monthly-mean observations have been obtained from the European Space Agency Climate Change Initiative (ESA CCI) sea level product version 2.0 (Ablain et al. 2015). The gridded estimates are averaged over each ocean basin to obtain basin-mean estimates.

3. Contributors to sea level and land-level changes

Sea level and land-level changes are caused by a multitude of processes, which all have their own temporal and spatial characteristics. In this section, we discuss the used estimates of the various processes affecting sea level changes.

Past and present-day mass exchange between land and ocean not only leads to changes in the global ocean volume, but as a result of changes in the earth rotation, gravity field, and deformation of the solid earth, local and regional sea level change can differ from the global-mean barystatic response. The combination of gravitational and earth-deformation effects causes a distinct regional sea level response pattern to mass exchange between land and ocean (Clark and Lingle 1977; Mitrovica et al. 2001; Bamber and Riva 2010). The local sea level response to mass redistribution can be separated in three individual components:

$$\eta(\theta,\phi,t) = G(\theta,\phi,t) - R(\theta,\phi,t) + \mathcal{L}(t), \qquad (1)$$

where $\eta(\theta, \phi, t)$ is the resulting local relative sea level anomaly from the mass change, $G(\theta, \phi, t)$ is the deformation of the geoid, $R(\theta, \phi, t)$ the solid earth deformation, and $\mathcal{L}(t)$ is a global-mean term, which is required to ensure mass conservation between continents and oceans. The term $\eta(\theta, \phi, t)$ expresses local sea level changes relative to the solid earth, which implies that deformation of the solid earth will be part of local relative sea level changes. We solve Eq. (1) for present-day mass exchange using the elastic sea level equation (Tamisiea et al. 2010), with the method described by Sabadini et al. (2016) to compute the earth rotational feedback.

For GIA, we use output from the global ICE6G_VM5a model (Peltier et al. 2015), which provides estimates of both changes in the geoid, solid earth, and relative sea level due to GIA.

For present-day mass redistribution, we include the effects of glacier and ice sheet mass loss, dam retention, and groundwater depletion, for which the same estimates as in Frederikse et al. (2017) are used. We will discuss these estimates briefly. Glacier mass loss is based on data from Marzeion et al. (2015), which provides mass balance evolution estimates for the 18 major glacier-covered regions. For the Greenland Ice Sheet, we use the total mass balance estimates and the accompanying uncertainties of Kjeldsen et al. (2015) between 1958 and 1992. Between 1992 and 2014, the mass balance is based on RACMO2.3 for the surface mass balance (SMB), while ice discharge is modeled using a constant acceleration of 6.6 Gt yr^{-2}, following van den Broeke et al. (2016). The Antarctic contribution is less certain, especially before the 1990s, because of the sparse observations during the presatellite era. However, from earth rotation observations it can be inferred that the Antarctic contribution before the 1990s has been small (Mitrovica et al. 2015). Therefore, we assume no mass change before 1979. Between 1979 and 1993, we adopt a long-term balance between the Antarctic Ice Sheet SMB, based on RACMO2.3 (van Wessem et al. 2014) and ice discharge between 1979 and 1993. After 1993, we impose an 2.0 Gt yr^{-2} acceleration of the ice discharge, which gives a reasonable fit to both the results of the IMBIE intercomparison case (Shepherd et al. 2012) and GRACE observations of ice-mass loss over more recent years (e.g., Watkins et al. 2015). Terrestrial water storage (TWS) changes are based on the effects of

groundwater depletion and dam retention. Groundwater depletion is based on PCRaster Global Water Balance (PCR-GLOBWB) model outcomes (Wada et al. 2014), multiplied by a correction factor of 0.8 to account for depleted groundwater that does not reach the ocean (Wada et al. 2016). Note that we only compute the large-scale solid-earth response to groundwater depletion, and local groundwater depletion results in uplift due to a decrease of the load. Local subsidence due to sediment compaction after groundwater withdrawal is thus not modeled by the TWS term. On local scales, this effect can be substantial (Chaussard et al. 2013; Minderhoud et al. 2017). Dam retention estimates are based on the GRanD (Global Reservoir and Dam) database (Lehner et al. 2011), which provides the location, storage capacity, and year of construction. Filling and seepage rates are estimated following the method of Chao et al. (2008). We refer to Frederikse et al. (2016) for a full description of the derivation of the present-day mass effects and the accompanying uncertainties. Figure S1 in the online supplemental information shows the resulting linear relative sea level trends of all aforementioned present-day mass processes.

Satellite altimetry does not detect solid earth deformation, since it observes sea level in a geocentric reference frame. Therefore, to compare altimetry to tide-gauge observations, we have to account for the deformation of the solid earth and put the observations in a relative reference frame. To do so, we subtract the modeled solid earth deformation due to GIA and present-day mass transport from the observed altimetry before the gridded altimetry estimates are averaged.

Next to changes in the ocean mass and the ongoing response to GIA, changes in steric height are a major contributor to global sea level changes. We use gridded estimates of in situ observations of temperature and salinity to compute the resulting steric height changes. These estimates are obtained from the EN4 version 4.1.1 gridded temperature and salinity dataset (www.metoffice.gov.uk/hadobs/en4/; Good et al. 2013). From the gridded estimates of temperature and salinity, density anomalies are computed, which are converted into steric height anomalies, using the seawater properties described in Roquet et al. (2015). The density and steric height anomalies have been computed using the TEOS-10 (Thermodynamic Equation of Seawater 2010) software (McDougall and Barker 2011). To obtain an estimate of the accompanying uncertainty, we have computed steric heights from other datasets, and use the spread between the different estimates as a measure of the uncertainty. We have used gridded temperature and salinity datasets from Ishii and Kimoto (2009), and the temperature-only dataset from Cheng and Zhu (2016), as well as the pentadal steric height estimates from Levitus et al. (2012). We use the upper 2000 m of the ocean in all datasets, except for that of Ishii and Kimoto (2009), which only covers the upper 1500 m. The gridded fields are averaged over the individual basins to obtain estimates of basin-mean and global steric changes.

The time series of the sea level effect of GIA, present-day mass redistribution, and the steric contribution, together with an estimate of their uncertainties, are depicted in Fig. 3. An overview of the individual contributors to the present-day mass redistribution term is shown in Fig. S2. In general, the steric signal varies substantially from basin to basin, and dominates the variability signal, while the present-day mass redistribution terms are mostly showing changes over longer time scales. In the subtropical and subpolar North Atlantic ocean, GIA causes an upward trend, which is nearly absent in other basins and in the global mean. Furthermore, these regions have a smaller contribution from present-day mass redistribution, due to their proximity to the Greenland Ice Sheet and many glacier-covered regions. The below-average contribution of mass-related processes to sea level changes in the North Atlantic has as a consequence that the accelerating contributions from the Greenland Ice Sheet and many glacier-covered regions to sea level are less observable in this basin. Many of the world's longest tide-gauge records are located in this basin, which could be a major factor in the difficulty to detect an acceleration in global-mean sea level from tide-gauge records. Furthermore, it can be noticed that the spread in estimates of steric changes is substantially larger in the Atlantic basins, compared to all other basins, despite the relatively high coverage of hydrographic profiles in the North Atlantic Ocean (e.g., Cheng and Zhu 2016).

4. A local sea level budget

The sea level change fields that result from combining GIA, present-day mass redistribution, and steric height can be sampled at each tide-gauge location. However, since many tide-gauge locations are located on shallow shelves, the steric signal will vanish when the signal is sampled at the coast, and local sea level variability at most tide-gauge locations is associated with ocean-bottom pressure changes (Landerer et al. 2007). Furthermore, because of the presence of finescale coastal and boundary dynamics, sampling the steric height field in the open ocean close to the tide-gauge location will not provide information about local ocean dynamics, since the observations are averaged over large spatial distances (Bingham and Hughes 2012; Good et al. 2013). These issues imply that sampling the steric field at or

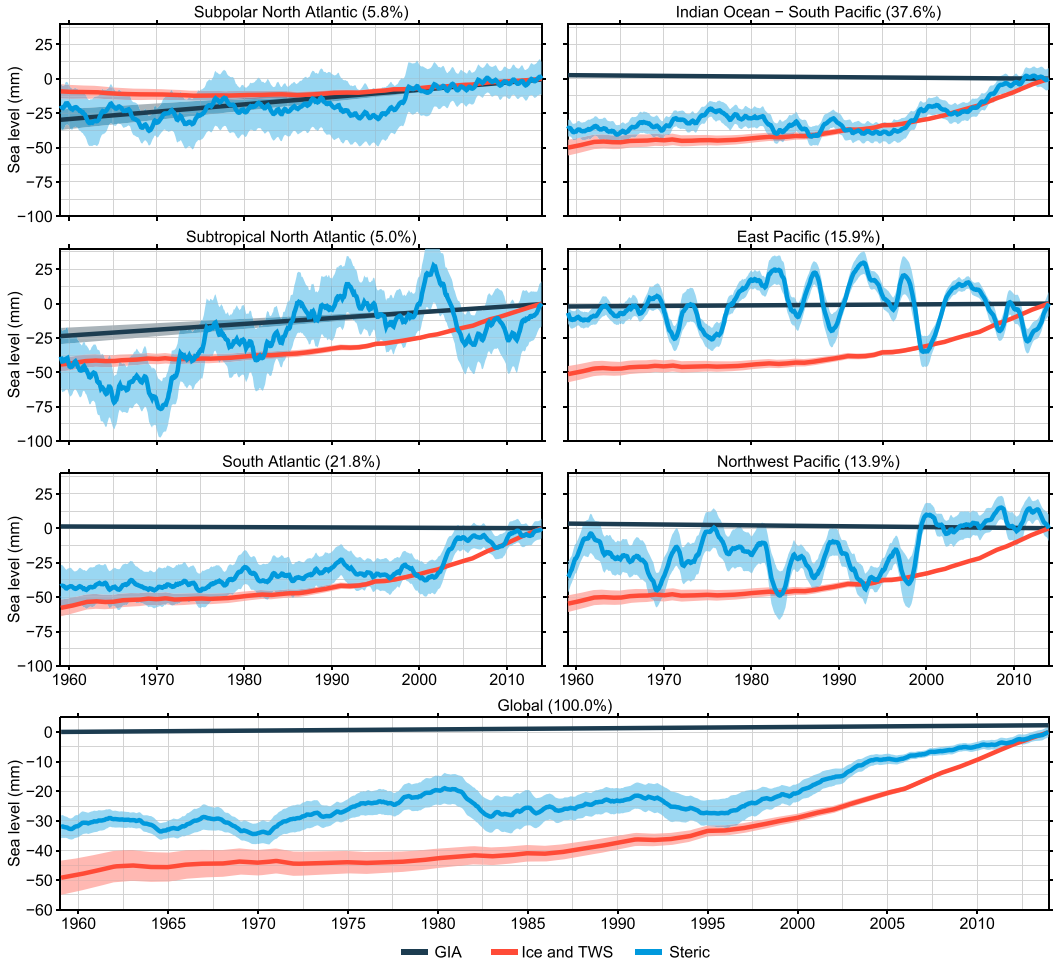

FIG. 3. Contributors to basin-mean and global sea level changes. The mass contribution consists of the sum of the glacier, Greenland Ice Sheet, Antarctic Ice Sheet, and terrestrial water storage contribution. The shading denotes an estimate of the confidence interval on the 1σ level. All time series have been low-pass filtered using a 25-month running mean. The percentages in the headers show the fraction of the global ocean covered by each basin.

close to the tide-gauge location will not provide a reliable estimate of the impact of ocean dynamics on local sea level. Hence, we use the basin-mean steric estimate as proxy for the local effect of steric changes on tide gauges. This approximation implies that local ocean dynamic effects on sea level are excluded. These local effects often lead to distinct trends, such as the strong acceleration along the northwestern Atlantic coast (Sallenger et al. 2012). Therefore, local ocean dynamics are a likely candidate to explain the difference between observed sea level and our sum of contributors.

Local relative sea level changes from GIA and present-day mass exchange are partially caused by VLM due to solid-earth deformation, as shown in Eq. (1). The contribution of present-day mass exchange is not linear over the study period, and because the VLM trends are not necessarily derived over the same period as the tide-gauge trends, the observed VLM trend may not be representative for the full tide-gauge record (Riva et al. 2017). To avoid this bias, we use the method of Frederikse et al. (2016) to separate the observed VLM in a part explained by GIA and present-day mass effects and an unexplained part:

$$\frac{d\overline{z}_r}{dt} = \frac{d\overline{z}}{dt} - \frac{d\overline{R}_{\mathrm{GIA}}}{dt} - \frac{d\overline{R}_{\mathrm{PD}}}{dt}, \tag{2}$$

where $d\overline{z}_r/dt$ is the unexplained part of the VLM trend, $d\overline{z}/dt$ is the observed linear VLM trend, $d\overline{R}_{\mathrm{GIA}}/dt$ is the modeled linear VLM trend resulting from GIA, and $d\overline{R}_{\mathrm{PD}}/dt$ is the linear trend in solid earth deformation resulting from present-day mass redistribution over the period covered by the VLM observation at each station. Since this linear trend is only computed over the time

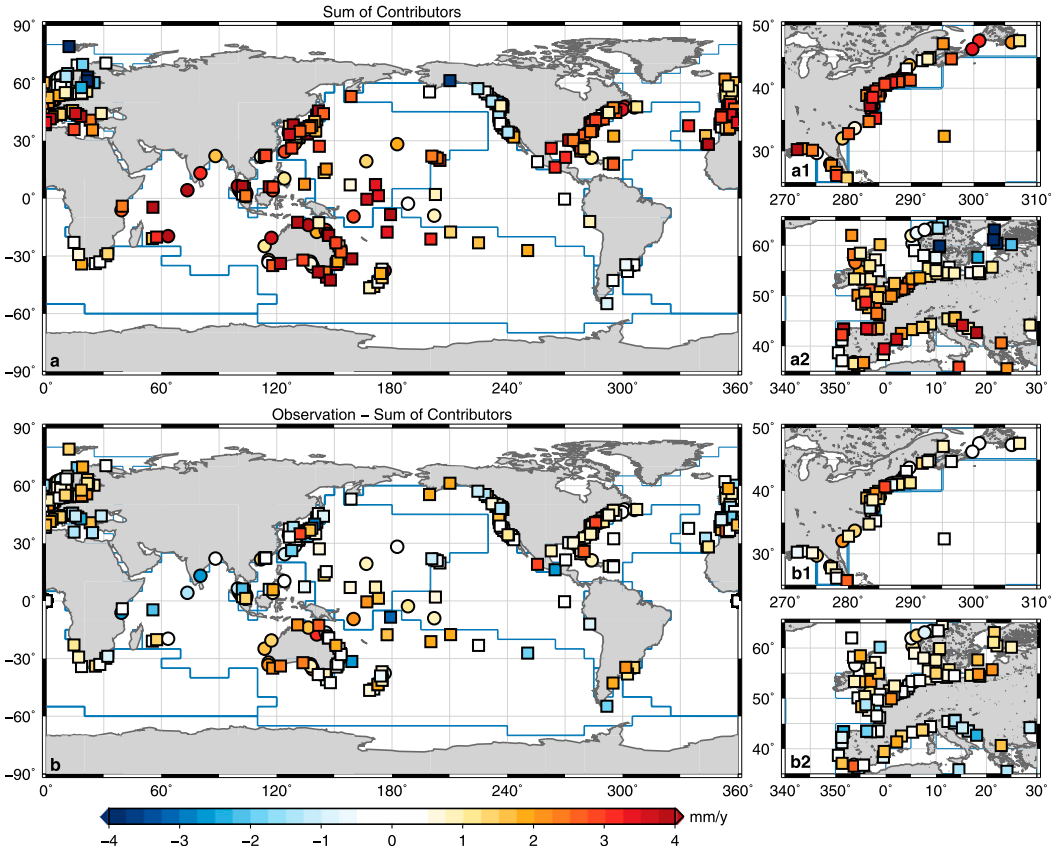

FIG. 4. Modeled trends for the individual stations. (a) Sum of contributors per station, computed as in Eq. (3). (b) Observed trends in tide-gauge records (not corrected for VLM or residual VLM) minus the sum of contributors. The smaller panels on the right (labeled a1, a2, b1, and b2) are zoom-ins of (a) and (b) along the densely sampled European and American Atlantic coasts. The blue lines depict the boundaries of the individual basins.

span of the VLM observations, its value differs from the trend over the tide-gauge observation epoch. We assume the unexplained VLM signal $d\overline{z}_r/dt$ to be constant over the whole time span of the tide-gauge observations. With this approach, we account for the nonlinear VLM associated with solid-earth deformation resulting from present-day mass redistribution.

The average rate of VLM is $-0.08\,\mathrm{mm\,yr^{-1}}$ with a standard deviation of $1.49\,\mathrm{mm\,yr^{-1}}$. After removing the known terms, the average residual VLM becomes $-0.11\,\mathrm{mm\,yr^{-1}}$ with a standard deviation of $1.05\,\mathrm{mm\,yr^{-1}}$. Hence, on average, the tide gauges are not subject to large VLM signals before and after correcting for known processes that cause VLM. Since a substantial part of the tide-gauge stations are located in areas subject to GIA-related uplift, the distribution of the VLM trends may be skewed: if we compare the median trends, we do find a reduction from $-0.28\,\mathrm{mm\,yr^{-1}}$ for the median VLM trend to $-0.13\,\mathrm{mm\,yr^{-1}}$ for the median residual VLM trend. However, the standard deviation of uncorrected and residual VLM is still substantial. Histograms of the uncorrected and residual rates of VLM per basin are shown in Fig. S3.

We use the estimate of VLM that is unrelated to both GIA and present-day mass transport only to correct for unknown local VLM. Hence, we can use the relative sea level changes $\eta(\theta, \phi, t)$ resulting from GIA and present-day mass transport to compute the local sum of contributors. We define the local sum of contributors as follows:

$$\eta_{\mathrm{Sum}}(t) = \eta_{\mathrm{GIA}}(t) + \eta_{\mathrm{PD}}(t) + \eta_{\mathrm{Steric}}(t) - \overline{z}_r(t), \quad (3)$$

where $\eta_{\mathrm{Sum}}(t)$ is the sum of contributors; $\eta_{\mathrm{GIA}}(t)$ and $\eta_{\mathrm{PD}}(t)$ are the contributions of GIA and present-day mass redistribution, and $\eta_{\mathrm{Steric}}(t)$ is the steric height contribution, averaged over the basin to which the tide gauge is tied. The resulting sum of contributors per station is depicted in Fig. 4a.

The figure shows that the sum of contributors shows considerable variability with some distinct regional features: High rates are found around Australia and the

northwest Atlantic, while low rates can be found along the east coast of the Pacific and Fennoscandia. The residual tide-gauge signal (η_{Residual}) can now be expressed as the difference between observed sea level (η_{Obs}) and the sum of contributors:

$$\eta_{\text{Residual}}(t) = \eta_{\text{Obs}}(t) - \eta_{\text{Sum}}(t). \quad (4)$$

The linear trend in the residual tide gauge signal for all individual stations is shown in Fig. 4b. We see that many stations only show a small residual tide-gauge trend. However, in some regions, especially around Western Australia, the tide-gauge observations show a higher trend than explained by the sum of contributors. Around Western Australia, the alongshore propagation of multidecadal wind-driven variability (Feng et al. 2004) may be one of the causes for this deviation.

The mean trend observed by the stations is 1.88 mm yr^{-1}, with a standard deviation of 1.74 mm yr^{-1}. This mean trend is larger than the mean trend of the sum of contributors sampled at the tide-gauge locations, which is 1.52 mm yr^{-1} with a standard deviation of 1.68 mm yr^{-1}. Also for each individual basin, the observed trends are on average higher than the sum of contributors. This global and basin-mean difference is also found when instead of the mean, the median observed trend and sum of contributors is used. Figure S4 shows global and basin-mean histograms of the observed trends and sum of processes. This difference may show that the sum of contributors underestimates the trend in global-mean sea level rise. However, the spatial sampling of the tide gauges is uneven, which could result in some oversampled regions, leading to biases when the observations are simply averaged without weighing. In the next section, we will discuss a reconstruction of basin-scale and global-scale sea level changes where we show that this difference between observed sea level and the sum of contributors is affected by the uneven spatial sampling and becomes smaller in the reconstructed basin-mean and global fields.

5. A basin-mean and global sea level reconstruction

Since tide-gauge observations are not evenly sampled over each basin, and because no common datum exists for tide gauges (Ray and Douglas 2011), we cannot simply average the tide-gauge records over their overlapping period. To overcome this spatial and temporal sampling problem, we reconstruct sea level changes in each basin from individual tide-gauge records using the virtual station technique (Jevrejeva et al. 2006, 2014). The virtual station technique recursively combines the two nearest stations to form a new virtual station halfway both stations. This procedure is repeated until only one station is left, which is used as the final estimate of sea level changes over the basin. To overcome the problem of an unknown common datum, one could either obtain an empirical common datum or use first differences to remove the datum problem. Dangendorf et al. (2017) show that estimating a common datum when averaging two stations can be done by requiring both stations to share a minimum common observation time span. The average sea level of both stations over the common period is removed before both time series are averaged. They show using synthetic sea level data that this procedure results in a more reliable estimate than using first differences. We also use this common datum, where we require the stations to have an overlap length of at least 240 months.

To reduce the bias that occurs when the spatially and temporally varying sea level field is sampled at tide-gauge locations, we correct for the spatial effects due to GIA, present-day mass redistribution, and residual VLM. We first compute the difference between the local and basin-mean relative sea level change due to GIA and present-day mass redistribution, and remove this difference. We also remove the residual VLM at this stage. With these corrections, we make a best guess of basin-mean sea level from an individual tide-gauge record, since the known local deviations from basin-mean sea level are removed. The corrected tide-gauge (tg) observation time series of each station then reads as follows:

$$\eta_{\text{basin}} = \eta_{\text{tg}} + \overline{Z_r} + (\eta_{\text{GIA,basin}} - \eta_{\text{GIA,tg}}) + (\eta_{\text{PD,basin}} - \eta_{\text{PD,tg}}), \quad (5)$$

where η_{basin} is the estimate of the basin-mean sea level, based on a single tide-gauge time series; $\overline{Z_r}$ is the residual VLM term defined in Eq. (2); and $(\eta_{\text{GIA,basin}} - \eta_{\text{GIA,tg}})$ is the negative local deviation from the basin-mean GIA signal, which is added to the basin-mean estimate, to minimize the sampling bias. Note that $(\eta_{\text{PD,basin}} - \eta_{\text{PD,tg}})$ is the same deviation, but for the present-day mass transport terms.

We compute η_{Basin} for each station in a basin, and subsequently compute the basin-mean estimate by applying the aforementioned virtual station technique, with the corrected η_{basin} term as input. Applying Eq. (5) to all tide-gauge records reduces the standard deviation of the observed tide-gauge trends from 1.74 to 1.47 mm yr^{-1}.

To obtain estimates of the uncertainties of our reconstructed basin estimates, we compute a Monte Carlo estimate by generating surrogate time series for each station. To do so, we assume that the autocorrelated noise signal of tide gauges can be approximated by a power-law noise process. First, the properties of the

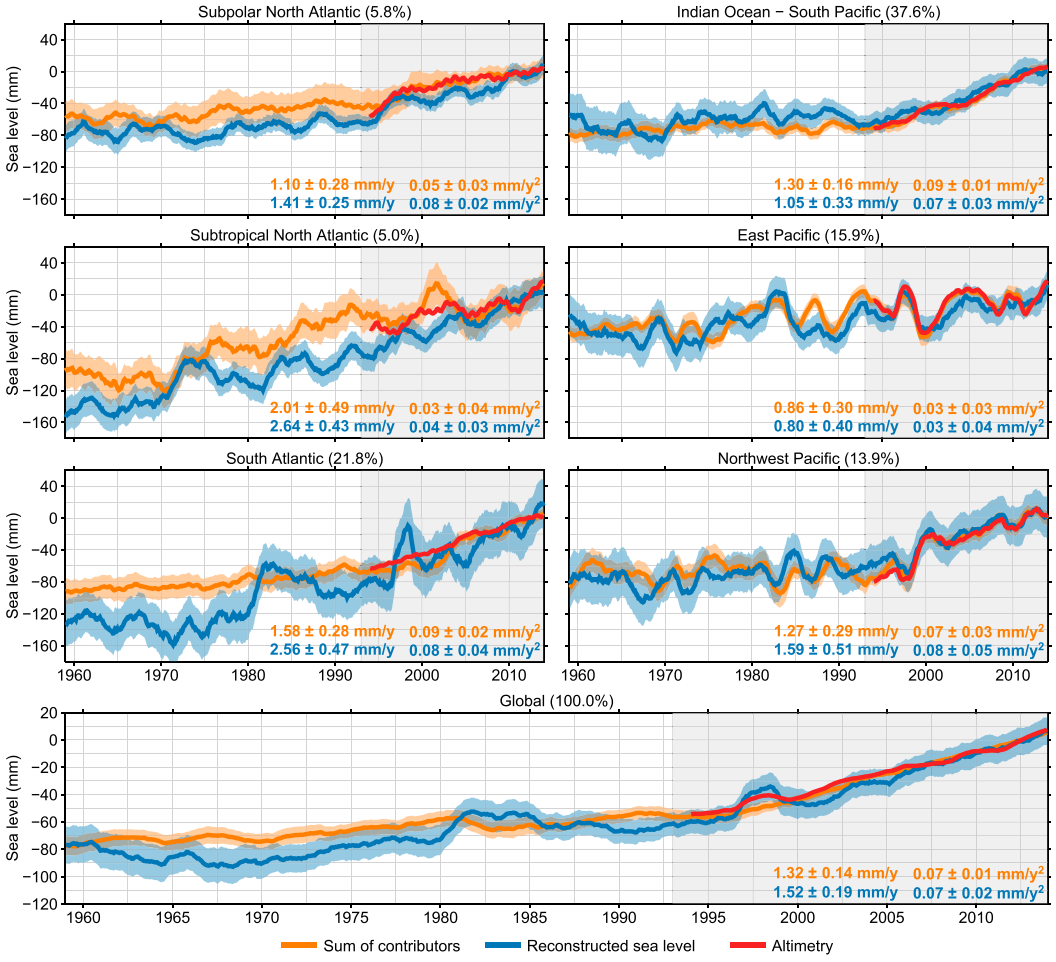

FIG. 5. Reconstructed basin-mean and global sea level, together with the sum of contributors. All time series have been low-pass filtered using a 25-month moving average filter. The colored shadings denote the estimated confidence intervals. The confidence intervals for the trends, accelerations, and time series are on the 1σ level. The gray shading denotes the epoch (1993–2014) over which the mean of each time series has been removed.

power-law noise are estimated using a maximum-likelihood approach (Bos et al. 2013). Then, surrogate noise time series with the same length, gaps, and noise properties as the original time series are generated using the method from Kasdin (1995). The noise property estimation and the generation of surrogate time series are performed using the Hector software (Bos et al. 2013). Each surrogate noise time series is augmented with a linear trend, whose slope is generated from a normal distribution based on the standard error of the VLM term. The virtual station method is repeated 1000 times with the surrogate data, from which estimates of the confidence interval for the linear trend, acceleration, and time series are computed. Note that the spatial correlation between tide gauges is not taken into account when estimating the surrogate noise series. Hence, the obtained uncertainties may underestimate the real uncertainty in regions where the tide-gauge observations are spatially correlated.

The global reconstruction is based on the average of all basins, weighted by the area of each basin. The associated uncertainties are also computed from the basin-mean surrogate time series. The resulting reconstructions are shown in Fig. 5, together with the sum of contributors. The first observation that can be made is that for all regions, the reconstructed sea level trends and accelerations are in agreement with the sum of contributors within $1-\sigma$ intervals. The exception is the South Atlantic basin, where the observed sea level trend is larger than the sum of contributors. In the Pacific and Indian Ocean, the reconstructed sea level variability is in broad agreement with the sum of contributors and altimetry, while in all Atlantic basins the observed decadal

TABLE 1. Trends and accelerations over 1958–2014 in individual contributors and their sum. The confidence interval is at the 1σ level.

	Trend (mm yr^{-1})	Acceleration (mm yr^{-2})
Glaciers	0.49 ± 0.03	0.011 ± 0.001
Greenland ice sheet	0.21 ± 0.02	0.007 ± 0.001
Antarctic ice sheet	0.06 ± 0.03	0.007 ± 0.001
Terrestrial water storage	−0.02 ± 0.09	0.019 ± 0.003
Present-day mass	0.74 ± 0.10	0.044 ± 0.004
Steric	0.54 ± 0.10	0.026 ± 0.011
GIA	0.04 ± 0.01	
Sum of contributors	1.32 ± 0.14	0.070 ± 0.011
Reconstructed GMSL	1.52 ± 0.19	0.067 ± 0.018

variability is not reproduced by the contributors. In the South Atlantic basin, where the difference is the most substantial, this discrepancy could be caused by the low number of observations in this region, which may result in the propagation of local variability at a limited number of locations into the basin-mean reconstruction. In the other Atlantic basins, the data coverage, both from tide gauges and hydrographic observations, is generally high. A possible explanation of the discrepancy in these basins may be the decoupling between open-ocean and boundary sea level variability, which is omnipresent in the Atlantic Ocean (Hughes and Meredith 2006), as well as the sea level signal that emerges from changes in the AMOC strength and Gulf Stream variability, which generate very localized sea level fingerprints (Ezer 2015). In the Pacific and Indian Oceans, many tide gauges are located at open-ocean islands, which are generally more representative for open-ocean sea level changes (Williams and Hughes 2013). Another possible explanation for the differences in the subtropical North Atlantic is nonlinear subsidence due to sediment compaction and groundwater depletion along the northern coast of the Gulf of Mexico, which is not fully quantified in the VLM records (Kolker et al. 2011).

The global-mean reconstruction, which is the average of the basin-mean signals, weighed by their areas, also shows some decadal variability that is absent in the sum of contributors. A part of this variability signal is likely caused by the unexplained variability in the South Atlantic ocean, since the phase of the unexplained variability signal coincides. Over the common period with altimetry observations, the reconstructed sea level, altimetry, and the sum of contributors are in good agreement.

The trends and accelerations of the individual contributors to sea level rise and their sum are shown in Table 1. The estimated trend in sum of contributors is $1.3 \pm 0.1\,\mathrm{mm\,yr^{-1}}$, which explains the reconstructed global-mean sea level trend of $1.5 \pm 0.2\,\mathrm{mm\,yr^{-1}}$ within the $1-\sigma$ confidence interval. Also, the acceleration in the sum of contributors ($0.07 \pm 0.01\,\mathrm{mm\,yr^{-2}}$) explains the reconstructed sea level acceleration of $0.07 \pm 0.02\,\mathrm{mm\,yr^{-2}}$. Note that the numbers in the table are not exactly equal to the equivalent barystatic mass changes, since some parts of the Arctic and Antarctic Oceans are not part of the ocean basins over which the modeled sea level change is averaged, as depicted in Fig. 1a. The acceleration in the sum of all present-day mass-redistribution processes is substantially larger than the acceleration in steric sea level. A positive acceleration is present in all individual basins, although in the east Pacific the acceleration is not significant.

6. Discussion

To assess whether our new approach for reconstructing global-mean sea level affects the resulting trend and variability, we computed the reconstruction, but with different corrections applied to the tide-gauge data before applying the virtual station method. In the ''no corrections'' run, the virtual station method is applied to the time series without any prior correction. In the ''GIA only'' run, we only remove the local relative sea level deviation from the basin mean from each individual tide-gauge record due to GIA before averaging. The ''present-day only'' run only applies the correction for present-day mass redistribution, and the ''no VLM'' run applies the GIA and present-day mass correction terms, but no VLM corrections. In the ''VLM only'' run, we remove the uncorrected linear VLM trend from each station. The results are depicted in Fig. 6. The figure shows that the choice of corrections applied to the tide-gauge data before merging them using the virtual station technique affects the resulting global-mean sea level trend. The effects of GIA, local VLM, and present-day mass redistribution each have a different impact on sea level reconstructions. The decadal variability does not show large differences between the reconstructions, which is not surprising, as the corrections applied to the tide-gauge stations are either linear (GIA, VLM, residual VLM) or only slowly varying (present-day mass transport) in nature. Compared to the use of uncorrected tide-gauge data, our corrections result in a small increase in estimated global mean sea level rise. The corrections for present-day mass redistribution and GIA both result in an increase of the reconstructed trend, compared to the uncorrected run. This increase is consistent with the results reported in Thompson et al. (2016), who also find that sampling spatial fingerprints of recent ice-mass loss at tide-gauge locations results in an

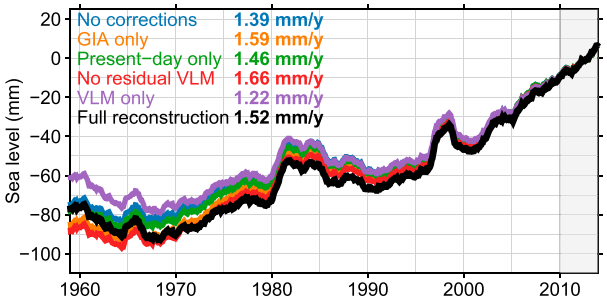

FIG. 6. Reconstruction of global-mean sea level, with different corrections applied to the tide-gauge records before applying the virtual station method. The mean value over the epoch marked by the gray bar (2009–14) has been removed from each reconstruction.

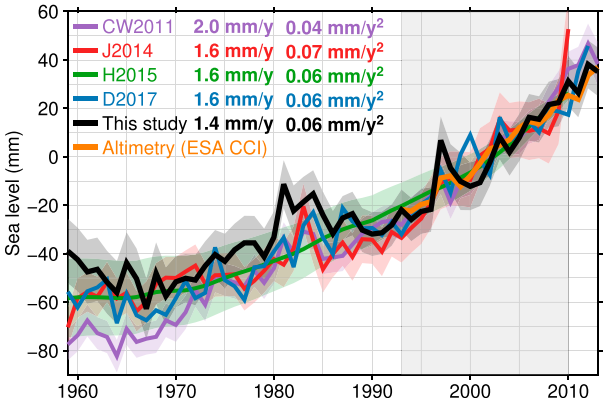

FIG. 7. A comparison of global mean sea level reconstructions based on tide-gauge observations from Church and White (2011), Jevrejeva et al. (2014), Hay et al. (2015), and Dangendorf et al. (2017), herein labeled CW2011, J2014, H2015, and D2017, respectively, and this study. The shading denotes the estimated confidence interval on the 1σ level. All reconstructions are resampled to annual-mean values. Central estimates of the trends and accelerations for all reconstructions are computed over 1958–2010.

underestimation of the accompanying barystatic sea level rise.

When the original VLM signal is removed from the tide gauges, the resulting trend decreases substantially. One of the reasons that may cause this large difference is that removing VLM from the tide-gauge records puts the reconstruction in a geocentric or absolute reference frame instead of a relative reference frame (Wöppelmann et al. 2009). Therefore, ocean-bottom deformation is removed from the sea level rise estimate. Hence, if the ocean bottom subsides, sea level relative to the ocean bottom will stay constant, but geocentric sea level will drop. It is well-known that GIA results in such an ocean-bottom motion signal, which leads to a reduction of 0.15–0.45 mm yr^{-1} of global geocentric sea level rise (Tamisiea 2011). Furthermore, present-day mass transport results in a higher pressure on the ocean bottom, and the latter will subside further as a response (Ray et al. 2013). Hence, some caution must be taken when correcting tide gauges for VLM, when one is interested in global mean sea level changes. The full reconstruction adds the residual VLM term to the corrections of GIA and present-day mass redistribution. The addition of residual VLM results in a lower GMSL estimate, despite the simple average residual VLM term is almost zero. An overview of the impact of the corrections for the sea level reconstruction on basin level is shown in Fig. S5.

Forward GIA models, including the ICE6G_VM5a model applied here, rely on estimates of the glaciation/deglaciation history and the viscosity structure of the earth, which are both difficult to constrain and prevent from estimating reliable uncertainties. Hence, specific choices made in the GIA model may affect the global and regional sum of contributors. To determine whether changing the underlying GIA model affects the sum of contributors, we have also run the analysis using the ICE6G_ANU model (Purcell et al. 2016) and the ICE5G_VM2 model (Peltier 2004). On a global scale, the differences are in the range of 0.04 mm yr^{-1}. In the subpolar and subtropical North Atlantic basins, differences on the order of 0.2 mm yr^{-1} occur, while outside these basins the differences are smaller. Figure S6 shows the effects of changing the GIA model on the estimate of the sum of contributors.

To assess how our reconstruction approach compares to other reconstructions, we have plotted our reconstruction together with the global reconstructions of Church and White (2011), Jevrejeva et al. (2014), Hay et al. (2015), and Dangendorf et al. (2017). Note that our reconstruction method is similar but not fully equal to the reconstruction method presented by Dangendorf et al. (2017): we use a different tide-gauge selection, a different GPS solution, and an alternative parameterization of the local deviations from the basin-mean sea level, as described in Eq. (5). The comparison between all reconstructions is depicted in Fig. 7. The figure shows that our reconstruction shows a slightly smaller increase in sea level than most reconstructions over the common period. To assess the significance of this difference, we computed the central estimates of the reconstructed trends in the above reconstructions over the common period (1958–2010). All central estimates are well within the 2σ range of our reconstruction, except for the reconstruction of Church and White (2011), which has a central value of 2.0 mm yr^{-1}. The central estimates of the accelerations of all reconstructions fall well within the 2σ range of our reconstruction. Over the altimetry era, all reconstructions show a consistent rise in sea level. Note that the reconstructed global sea level

acceleration over the period of this study (1958–2014) is higher than the acceleration found over the whole twentieth century (Hay et al. 2015; Dangendorf et al. 2017). This difference can be attributed to the different time spans, since we do not include the pre-1958 sea level changes, during which a sea level deceleration can be noted (Dangendorf et al. 2017).

7. Conclusions

We have computed estimates of sea level rise on a local, regional, and global scale over the last decades (1958–2014), and made an estimate of the sum of contributors to sea level changes. We have developed an updated approach to reconstruct global and basin-mean sea level by explicitly taking into account local VLM and the nonlinear effects of present-day mass redistribution on both tide-gauge and VLM observations in a consistent framework. Together with the use of a common mean to merge individual tide-gauge records, as described by Dangendorf et al. (2017), the resulting basin-mean trends and accelerations are in agreement with the sum of contributors in all basins, except for the sparsely observed South Atlantic. In the Indian and Pacific Oceans, the sum of contributors shows good agreement with the observed decadal variability, while for the Atlantic region the reconstructed variability is not explained by the contributors. The spread between steric sea level reconstructions is large in the Atlantic Ocean, which also applies to the well-observed North Atlantic Ocean. Therefore, to obtain a more thorough understanding of the global sea level budget, an assessment of the various observations in the Atlantic region is worthwhile.

When the basin-mean records are merged into a global reconstruction, we also find good agreement between the reconstructed trend and acceleration and the sum of contributors. Hence, the sea level budget between 1958 and 2014 can be reasonably closed without requiring a large contribution from the Antarctic Ice Sheet before the 1990s or a contribution from thermal expansion in the deep ocean below 2000 m. However, the reconstructed decadal variability cannot be reproduced, which is partially caused by the spread in the sparsely observed South Atlantic Ocean.

Next to attempts to rescue more tide-gauge records (e.g., Hogarth 2014), another approach to the issue of sparse observations may be the use of high-resolution ocean models and reanalyses. These models may help separating local variability from basin-mean changes, which could reduce the large spread between observed sea level changes at tide gauges and the local sum of contributors, for which the local effects of ocean dynamics are still unknown.

Acknowledgments. Tide-gauge data has been obtained from the Permanent Service for Mean Sea Level (www.psmsl.org). The pressure and wind fields from the 20th Century Reanalysis Project V2c have been obtained from NOAA Earth System Research Laboratory (www.esrl.noaa.gov/psd/data/gridded). The global ICE6G-VM5a model has been obtained from www.atmosp.physics.utoronto.ca/~peltier/. The MIDAS GPS velocities have been downloaded from Nevada Geodetic Laboratory (geodesy.unr.edu/). The ESA CCI v2.0 sea-level observations have been obtained from http://cci.esa.int/. The EN4 version 4.1.1 gridded temperature and salinity fields were obtained from the U.K. Met Office (www.metoffice.gov.uk/hadobs/en4/). The Ishii and Kimoto dataset has been downloaded from the Research Data Archive at the National Center for Atmospheric Research, Computational and Information Systems Laboratory (http://rda.ucar.edu/datasets/ds285.3/). The estimates from Levitus et al. (2012) were downloaded from www.nodc.noaa.gov/OC5/3M_HEAT_CONTENT/. The Cheng and Zhu (2016) data were downloaded from http://159.226.119.60/cheng/. The Hector software package (v1.6) has been downloaded from segal.ubi.pt/hector. Some figures have been produced using the Generic Mapping Tools. We thank Marta Marcos for sharing the VLM data based on Wöppelmann and Marcos (2016). TF and REMR acknowledge funding from the Netherlands Organisation for Scientific Research (NWO) VIDI Grant 864.12.012. SJ was funded by the Natural Environmental Research Council under Grant Agreement NE/P01517/1.

REFERENCES

Ablain, M., and Coauthors, 2015: Improved sea level record over the satellite altimetry era (1993–2010) from the Climate Change Initiative project. *Ocean Sci.*, **11**, 67–82, https://doi.org/10.5194/os-11-67-2015.

Bamber, J., and R. E. M. Riva, 2010: The sea level fingerprint of recent ice mass fluxes. *Cryosphere*, **4**, 621–627, https://doi.org/10.5194/tc-4-621-2010.

Bingham, R. J., and C. W. Hughes, 2012: Local diagnostics to estimate density-induced sea level variations over topography and along coastlines. *J. Geophys. Res.*, **117**, C01013, https://doi.org/10.1029/2011JC007276.

Blewitt, G., C. Kreemer, W. C. Hammond, and J. Gazeaux, 2016: MIDAS robust trend estimator for accurate GPS station velocities without step detection. *J. Geophys. Res. Solid Earth*, **121**, 2054–2068, https://doi.org/10.1002/2015JB012552.

Bos, M. S., R. M. S. Fernandes, S. D. P. Williams, and L. Bastos, 2013: Fast error analysis of continuous GNSS observations with missing data. *J. Geod.*, **87**, 351–360, https://doi.org/10.1007/s00190-012-0605-0.

Chambers, D. P., A. Cazenave, N. Champollion, H. Dieng, W. Llovel, R. Forsberg, K. von Schuckmann, and Y. Wada, 2017: Evaluation of the global mean sea level budget between 1993 and 2014. *Surv. Geophys.*, **38**, 309–327, https://doi.org/10.1007/s10712-016-9381-3.

Chao, B. F., Y. H. Wu, and Y. S. Li, 2008: Impact of artificial reservoir water impoundment on global sea level. *Science*, **320**, 212–214, https://doi.org/10.1126/science.1154580.

Chaussard, E., F. Amelung, H. Abidin, and S.-H. Hong, 2013: Sinking cities in Indonesia: ALOS PALSAR detects rapid subsidence due to groundwater and gas extraction. *Remote Sens. Environ.*, **128**, 150–161, https://doi.org/10.1016/j.rse.2012.10.015.

Cheng, L., and J. Zhu, 2016: Benefits of CMIP5 multimodel ensemble in reconstructing historical ocean subsurface temperature variations. *J. Climate*, **29**, 5393–5416, https://doi.org/10.1175/JCLI-D-15-0730.1.

Church, J. A., and N. J. White, 2011: Sea-level rise from the late 19th to the early 21st century. *Surv. Geophys.*, **32**, 585–602, https://doi.org/10.1007/s10712-011-9119-1.

——, and Coauthors, 2011: Revisiting the Earth's sea-level and energy budgets from 1961 to 2008. *Geophys. Res. Lett.*, **38**, L18601, https://doi.org/10.1029/2011GL048794.

Clark, J. A., and C. S. Lingle, 1977: Future sea-level changes due to west Antarctic ice sheet fluctuations. *Nature*, **269**, 206–209, https://doi.org/10.1038/269206a0.

Compo, G. P., and Coauthors, 2011: The Twentieth Century Reanalysis Project. *Quart. J. Roy. Meteor. Soc.*, **137**, 1–28, https://doi.org/10.1002/qj.776.

Dangendorf, S., C. Mudersbach, T. Wahl, and J. Jensen, 2013: Characteristics of intra-, inter-annual and decadal sea-level variability and the role of meteorological forcing: The long record of Cuxhaven. *Ocean Dyn.*, **63**, 209–224, https://doi.org/10.1007/s10236-013-0598-0.

——, M. Marcos, G. Wöppelmann, C. P. Conrad, T. Frederikse, and R. Riva, 2017: Reassessment of 20th century global mean sea level rise. *Proc. Natl. Acad. Sci. USA*, **114**, 5946–5951, https://doi.org/10.1073/pnas.1616007114.

Ezer, T., 2015: Detecting changes in the transport of the Gulf Stream and the Atlantic overturning circulation from coastal sea level data: The extreme decline in 2009–2010 and estimated variations for 1935–2012. *Global Planet. Change*, **129**, 23–36, https://doi.org/10.1016/j.gloplacha.2015.03.002.

Feng, M., Y. Li, and G. Meyers, 2004: Multidecadal variations of Fremantle sea level: Footprint of climate variability in the tropical Pacific. *Geophys. Res. Lett.*, **31**, L16302, https://doi.org/10.1029/2004GL019947.

Frederikse, T., R. Riva, M. Kleinherenbrink, Y. Wada, M. van den Broeke, and B. Marzeion, 2016: Closing the sea level budget on a regional scale: Trends and variability on the northwestern European continental shelf. *Geophys. Res. Lett.*, **43**, 10 864–10 872, https://doi.org/10.1002/2016GL070750.

——, K. Simon, C. A. Katsman, and R. Riva, 2017: The sea-level budget along the northwest Atlantic coast: GIA, mass changes, and large-scale ocean dynamics. *J. Geophys. Res. Oceans*, **122**, 5486–5501, https://doi.org/10.1002/2017JC012699.

Good, S. A., M. J. Martin, and N. A. Rayner, 2013: EN4: Quality controlled ocean temperature and salinity profiles and monthly objective analyses with uncertainty estimates. *J. Geophys. Res. Oceans*, **118**, 6704–6716, https://doi.org/10.1002/2013JC009067.

Gregory, J. M., and Coauthors, 2013: Twentieth-century global-mean sea level rise: Is the whole greater than the sum of the parts? *J. Climate*, **26**, 4476–4499, https://doi.org/10.1175/JCLI-D-12-00319.1.

Hamlington, B. D., and P. R. Thompson, 2015: Considerations for estimating the 20th century trend in global mean sea level. *Geophys. Res. Lett.*, **42**, 4102–4109, https://doi.org/10.1002/2015GL064177.

——, ——, W. C. Hammond, G. Blewitt, and R. D. Ray, 2016: Assessing the impact of vertical land motion on twentieth century global mean sea level estimates. *J. Geophys. Res. Oceans*, **121**, 4980–4993, https://doi.org/10.1002/2016JC011747.

Hay, C. C., E. Morrow, R. E. Kopp, and J. X. Mitrovica, 2015: Probabilistic reanalysis of twentieth-century sea-level rise. *Nature*, **517**, 481–484, https://doi.org/10.1038/nature14093.

——, ——, ——, and ——, 2017: On the robustness of Bayesian fingerprinting estimates of global sea level change. *J. Climate*, **30**, 3025–3038, https://doi.org/10.1175/JCLI-D-16-0271.1.

Hill, E. M., J. L. Davis, M. E. Tamisiea, and M. Lidberg, 2010: Combination of geodetic observations and models for glacial isostatic adjustment fields in Fennoscandia. *J. Geophys. Res.*, **115**, B07403, https://doi.org/10.1029/2009JB006967.

Hogarth, P., 2014: Preliminary analysis of acceleration of sea level rise through the twentieth century using extended tide gauge data sets (August 2014). *J. Geophys. Res. Oceans*, **119**, 7645–7659, https://doi.org/10.1002/2014JC009976.

Holgate, S. J., and Coauthors, 2013: New data systems and products at the permanent service for mean sea level. *J. Coastal Res.*, **29**, 493–504, https://doi.org/10.2112/JCOASTRES-D-12-00175.1.

Hughes, C. W., and M. P. Meredith, 2006: Coherent sea-level fluctuations along the global continental slope. *Philos. Trans. Roy. Soc. London*, **364A**, 885–901, https://doi.org/10.1098/rsta.2006.1744.

Ishii, M., and M. Kimoto, 2009: Reevaluation of historical ocean heat content variations with time-varying XBT and MBT depth bias corrections. *J. Oceanogr.*, **65**, 287–299, https://doi.org/10.1007/s10872-009-0027-7.

Jevrejeva, S., A. Grinsted, J. C. Moore, and S. Holgate, 2006: Nonlinear trends and multiyear cycles in sea level records. *J. Geophys. Res.*, **111**, C09012, https://doi.org/10.1029/2005JC003229.

——, J. C. Moore, A. Grinsted, A. P. Matthews, and G. Spada, 2014: Trends and acceleration in global and regional sea levels since 1807. *Global Planet. Change*, **113**, 11–22, https://doi.org/10.1016/j.gloplacha.2013.12.004.

Kasdin, N. J., 1995: Discrete simulation of colored noise and stochastic processes and $1/f^{\alpha}$ power law noise generation. *Proc. IEEE*, **83**, 802–827, https://doi.org/10.1109/5.381848.

Kjeldsen, K. K., and Coauthors, 2015: Spatial and temporal distribution of mass loss from the Greenland ice sheet since AD 1900. *Nature*, **528**, 396–400, https://doi.org/10.1038/nature16183.

Kolker, A. S., M. A. Allison, and S. Hameed, 2011: An evaluation of subsidence rates and sea-level variability in the northern Gulf of Mexico. *Geophys. Res. Lett.*, **38**, L21404, https://doi.org/10.1029/2011GL049458.

Landerer, F. W., J. H. Jungclaus, and J. Marotzke, 2007: Ocean bottom pressure changes lead to a decreasing length-of-day in a warming climate. *Geophys. Res. Lett.*, **34**, L06307, https://doi.org/10.1029/2006GL029106.

Lehner, B., and Coauthors, 2011: High-resolution mapping of the world's reservoirs and dams for sustainable river-flow management. *Front. Ecol. Environ.*, **9**, 494–502, https://doi.org/10.1890/100125.

Levitus, S., and Coauthors, 2012: World ocean heat content and thermosteric sea level change (0–2000 m), 1955–2010. *Geophys. Res. Lett.*, **39**, L10603, https://doi.org/10.1029/2012GL051106.

Marzeion, B., P. W. Leclercq, J. G. Cogley, and A. H. Jarosch, 2015: Brief communication: Global reconstructions of glacier mass change during the 20th century are consistent. *Cryosphere*, **9**, 2399–2404, https://doi.org/10.5194/tc-9-2399-2015.

McDougall, T. J., and P. M. Barker, 2011: Getting started with TEOS-10 and the Gibbs Seawater (GSW) Oceanographic Toolbox. SCOR/IAPSO WG127, 28 pp., http://teos-10.org/pubs/Getting_Started.pdf.

Minderhoud, P. S. J., G. Erkens, V. H. Pham, V. T. Bui, L. Erban, H. Kooi, and E. Stouthamer, 2017: Impacts of 25 years of groundwater extraction on subsidence in the Mekong delta, Vietnam. *Environ. Res. Lett.*, **12**, 064006, https://doi.org/10.1088/1748-9326/aa7146.

Mitrovica, J. X., M. E. Tamisiea, J. L. Davis, and G. A. Milne, 2001: Recent mass balance of polar ice sheets inferred from patterns of global sea-level change. *Nature*, **409**, 1026–1029, https://doi.org/10.1038/35059054.

——, C. C. Hay, E. Morrow, R. E. Kopp, M. Dumberry, and S. Stanley, 2015: Reconciling past changes in Earth's rotation with 20th century global sea-level rise: Resolving Munk's enigma. *Sci. Adv.*, **1**, e1500679, https://doi.org/10.1126/sciadv.1500679.

Moore, J. C., S. Jevrejeva, and A. Grinsted, 2011: The historical global sea-level budget. *Ann. Glaciol.*, **52**, 8–14, https://doi.org/10.3189/172756411799096196.

Peltier, W. R., 2004: Global glacial isostasy and the surface of the Ice-Age Earth: The ICE-5G (VM2) model and GRACE. *Annu. Rev. Earth Planet. Sci.*, **32**, 111–149, https://doi.org/10.1146/annurev.earth.32.082503.144359.

——, D. F. Argus, and R. Drummond, 2015: Space geodesy constrains Ice Age terminal deglaciation: The global ICE-6G_C (VM5a) model. *J. Geophys. Res. Solid Earth*, **120**, 450–487, https://doi.org/10.1002/2014JB011176.

Piecuch, C. G., S. Dangendorf, R. M. Ponte, and M. Marcos, 2016: Annual sea level changes on the North American northeast coast: Influence of local winds and barotropic motions. *J. Climate*, **29**, 4801–4816, https://doi.org/10.1175/JCLI-D-16-0048.1.

Purcell, A., P. Tregoning, and A. Dehecq, 2016: An assessment of the ICE6G_C (VM5a) glacial isostatic adjustment model. *J. Geophys. Res. Solid Earth*, **121**, 3939–3950, https://doi.org/10.1002/2015JB012742.

Ray, R. D., and B. C. Douglas, 2011: Experiments in reconstructing twentieth-century sea levels. *Prog. Oceanogr.*, **91**, 496–515, https://doi.org/10.1016/j.pocean.2011.07.021.

——, S. B. Luthcke, and T. van Dam, 2013: Monthly crustal loading corrections for satellite altimetry. *J. Atmos. Oceanic Technol.*, **30**, 999–1005, https://doi.org/10.1175/JTECH-D-12-00152.1.

Riva, R. E. M., T. Frederikse, M. A. King, B. Marzeion, and M. R. van den Broeke, 2017: Brief communication: The global signature of post-1900 land ice wastage on vertical land motion. *Cryosphere*, **11**, 1327–1332, https://doi.org/10.5194/tc-11-1327-2017.

Roquet, F., G. Madec, T. J. McDougall, and P. M. Barker, 2015: Accurate polynomial expressions for the density and specific volume of seawater using the TEOS-10 standard. *Ocean Modell.*, **90**, 29–43, https://doi.org/10.1016/j.ocemod.2015.04.002.

Sabadini, R., B. Vermeersen, and G. Cambiotti, 2016: *Global Dynamics of the Earth: Applications of Viscoelastic Relaxation Theory to Solid-Earth and Planetary Geophysics.* Springer, 364 pp., https://doi.org/10.1007/978-94-017-7552-6.

Sallenger, A. H., Jr., K. S. Doran, and P. A. Howd, 2012: Hotspot of accelerated sea-level rise on the Atlantic coast of North America. *Nat. Climate Change*, **2**, 884–888, https://doi.org/10.1038/nclimate1597.

Shepherd, A., and Coauthors, 2012: A reconciled estimate of ice-sheet mass balance. *Science*, **338**, 1183–1189, https://doi.org/10.1126/science.1228102; Corrigendum, **338**, 1539, https://doi.org/10.1126/science.338.6114.1539-a.

Slangen, A. B. A., R. S. W. van de Wal, Y. Wada, and L. L. A. Vermeersen, 2014: Comparing tide gauge observations to regional patterns of sea-level change (1961–2003). *Earth Syst. Dyn.*, **5**, 243–255, https://doi.org/10.5194/esd-5-243-2014.

——, J. A. Church, C. Agosta, X. Fettweis, B. Marzeion, and K. Richter, 2016: Anthropogenic forcing dominates global mean sea-level rise since 1970. *Nat. Climate Change*, **6**, 701–705, https://doi.org/10.1038/nclimate2991.

Tamisiea, M. E., 2011: Ongoing glacial isostatic contributions to observations of sea level change. *Geophys. J. Int.*, **186**, 1036–1044, https://doi.org/10.1111/j.1365-246X.2011.05116.x.

——, E. M. Hill, R. M. Ponte, J. L. Davis, I. Velicogna, and N. T. Vinogradova, 2010: Impact of self-attraction and loading on the annual cycle in sea level. *J. Geophys. Res.*, **115**, C07004, https://doi.org/10.1029/2009JC005687.

Thompson, P. R., and M. A. Merrifield, 2014: A unique asymmetry in the pattern of recent sea level change. *Geophys. Res. Lett.*, **41**, 7675–7683, https://doi.org/10.1002/2014GL061263.

——, B. D. Hamlington, F. W. Landerer, and S. Adhikari, 2016: Are long tide gauge records in the wrong place to measure global mean sea level rise? *Geophys. Res. Lett.*, **43**, 10 403–10 411, https://doi.org/10.1002/2016GL070552.

van den Broeke, M. R., E. M. Enderlin, I. M. Howat, P. Kuipers Munneke, B. P. Y. Noël, W. J. van de Berg, E. van Meijgaard, and B. Wouters, 2016: On the recent contribution of the Greenland ice sheet to sea level change. *Cryosphere*, **10**, 1933–1946, https://doi.org/10.5194/tc-10-1933-2016.

van Wessem, J. M., and Coauthors, 2014: Improved representation of east Antarctic surface mass balance in a regional atmospheric climate model. *J. Glaciol.*, **60**, 761–770, https://doi.org/10.3189/2014JoG14J051.

Wada, Y., D. Wisser, and M. F. P. Bierkens, 2014: Global modeling of withdrawal, allocation and consumptive use of surface water and groundwater resources. *Earth Syst. Dyn.*, **5**, 15–40, https://doi.org/10.5194/esd-5-15-2014.

——, M.-H. Lo, P. J.-F. Yeh, J. T. Reager, J. S. Famiglietti, R.-J. Wu, and Y.-H. Tseng, 2016: Fate of water pumped from underground and contributions to sea-level rise. *Nat. Climate Change*, **6**, 777–780, https://doi.org/10.1038/nclimate3001.

Watkins, M. M., D. N. Wiese, D.-N. Yuan, C. Boening, and F. W. Landerer, 2015: Improved methods for observing Earth's time variable mass distribution with GRACE using spherical cap mascons. *J. Geophys. Res. Solid Earth*, **120**, 2648–2671, https://doi.org/10.1002/2014JB011547.

Williams, J., and C. W. Hughes, 2013: The coherence of small island sea level with the wider ocean: A model study. *Ocean Sci.*, **9**, 111–119, https://doi.org/10.5194/os-9-111-2013.

Wöppelmann, G., and M. Marcos, 2016: Vertical land motion as a key to understanding sea level change and variability. *Rev. Geophys.*, **54**, 64–92, https://doi.org/10.1002/2015RG000502.

——, C. Letetrel, A. Santamaria, M.-N. Bouin, X. Collilieux, Z. Altamimi, S. D. P. Williams, and B. M. Miguez, 2009: Rates of sea-level change over the past century in a geocentric reference frame. *Geophys. Res. Lett.*, **36**, L12607, http://doi.org/10.1029/2009GL038720.